Advanced Materials Research *Online: 2014-08-11*
ISSN: 1662-8985, Vol. 996, pp 155-161
doi:10.4028/www.scientific.net/AMR.996.155

Determination of Stress Profiles in Expanded Austenite by Combining Successive Layer Removal and GI-XRD

Frederico A.P. Fernandes[1,a *], Thomas L. Christiansen[1,b] and Marcel A.J. Somers[1,c]

[1]Technical University of Denmark, Department of Mechanical Engineering, Kgs. Lyngby,Denmark

[a]frfer@mek.dtu.dk, [b]tch@mek.dtu.dk, [c]somers@mek.dtu.dk

Keywords: Low temperature surface hardening; Gas nitriding; Expanded austenite; X-ray diffraction; Stress analysis; Grazing incidence.

Abstract. The present work deals with the evaluation of the residual-stress profile in expanded-austenite by successive removal steps using GI-XRD. Preliminary results indicate stresses of several GPa's from 111 and 200 diffraction lines. These stresses appear largest for the 200 reflection. The strain-free lattice parameter decayed smoothly with depth, while for the compressive stress a maximum value is observed at some depth below the surface. Additionally a good agreement was found between the nitrogen profile determined with GDOES analysis and the strain-free lattice parameter from XRD.

Introduction

The transformation of the surface region of austenitic stainless steel into a case of expanded austenite is associated with a spectacular improvement of the wear and fatigue performance, while the general corrosion performance remains largely unaffected and the resistance against local corrosion (as pitting) is improved. Expanded austenite is obtained by dissolving colossal amounts of nitrogen and/or carbon into the austenite lattice [1,2] at a temperature that is too low to allow long range diffusion of substitutionally dissolved elements within the time span of the treatment. Accordingly, the depth of the hard case is entirely the result of (stress-assisted) interstitial ingress of carbon and/or nitrogen atoms in austenite. No new phase develops and expanded austenite should be considered as a solid solution zone (diffusion zone) in austenite. As a consequence of the high content of interstitially dissolved nitrogen and/or carbon huge compressive residual stress is built up along with the interstitial concentration gradient. Residual stress values of -7.5 GPa within the plane parallel to the surface have been reported for nitrided austenitic stainless steel; these huge values were obtained while probing the 200 expanded austenite reflection [3]. Plastic accommodation and associated relaxation of the enormous composition-induced stresses were manifested as grain push-out [4,5] lattice rotations [6] and enhanced stacking fault densities [4]. For carburized stainless steel the reported stress values amount to -2.7 GPa, also while probing the 200 expanded austenite reflection [7].

Surface layers obtained by thermochemical surface engineering can usually be assumed to experience a rotationally symmetric biaxial state of stress, implying that $\sigma_{11} = \sigma_{22} = \sigma_{//}$ which leads to a simplification of the dependence of the lattice strain, ε_{ψ}^{hkl}, for the family of lattice planes *{hkl}* on the tilt angle ψ [12].

Depth-resolved quantification of composition-induced stress profiles in expanded austenite with X-ray diffraction techniques is far from trivial, as in addition to a stress gradient, also gradients in composition and stacking-fault density affect the lattice spacing [7-10]. Both destructive and non-destructive measurement strategies and data correction procedures have been published in the latter years to unravel the contributions of stress, composition and stacking fault gradients on lattice spacing profiles in this system [7,9,10].

The application of an asymmetric path by grazing incidence allows X-rays to penetrate only a very shallow depth range under the exposed surface and, thus, minimizes the effect of lattice

spacing gradients in the probed depth on the diffracted intensity weighted lattice spacing and additionally no data correction procedure is necessary [11]. In the present contribution non-symmetrical X-ray diffraction at a fixed incident (grazing incidence) angle combined with successive layer removal is explored to determine (steep) stress and composition profiles in an expanded austenite case obtained by gaseous nitriding.

Another important consideration concerns the *hkl*-dependent X-ray elastic constants (XECs) which most certainly depend on the composition of expanded austenite. In principle, the XECs can be calculated from the single crystal elastic constants, adopting an appropriate grain interaction model (GIM) for the elastic interaction between constrained crystallites. However, the single crystal elastic constants of expanded austenite are yet unknown. Therefore, arbitrarily, hitherto the self-consistent Kröner-Eshelby model [13] was adopted and values reported for 12%Cr-12%Ni-Fe [14,15] were taken. The implications of choosing these XECs for 200 and 111 reflections of expanded austenite for relating the lattice strain to residual stress are discussed in this work.

Experimental

Sample preparation. Discs with a diameter of 20 mm and a thickness of 3 mm were cut from a solution heat-treated bar of AISI 316L with the following chemical composition: Fe- 0.019C- 0.067N- 1.47Mn- 0.40Si- 16.26Cr- 10.05Ni- 2.02Mo- 0.47Cu (wt-%). The flat surfaces of the specimens were ground and polished at a final step using 3µm diamond solution to achieve a mirror like surface finish.

Gaseous thermochemical treatments were conducted in a hermetic furnace with gas circulation at 430ºC for 20h applying 2L/min of pure ammonia (NH_3). Activation of the samples to remove the protective oxide layer was carried out in-situ prior to nitriding; the details of this pre-treatment are proprietary.

For metallographic investigation cross sections of the nitrided samples were hot mounted, followed by grinding and polishing for investigation in a Neophot 32 reflected light microscope. To reveal the microstructural features of the produced layers, Kalling's reagent 1 was employed for approximately 15s. The embedded cross sections were also used for measuring the Vickers micro-hardness profile with a Future Tech model FM-700 hardness tester, applying a load of 5gf and a dwell time of 5s.

Glow Discharge Optical Emission Spectroscopy (GDOES) using a Horiba Jobin Yvon GD profiler 2 was applied to determine the nitrogen-depth profile. The plasma applied for controlled sputtering of the sample surface during GDOES was created at a pressure of 1000 Pa and 40 W. Nitrogen-depth profiles, as well as contents of the substitutionally dissolved components, were obtained using a selection of stainless steel reference materials and γ'-Fe_4N on pure iron was taken as a nitrogen reference.

X-ray Diffraction experiments were performed using a Bruker AXS D8 diffractometer equipped with a Cr tube with a characteristic wavelength of 2.2897Å. The equipment was operated employing a voltage of 40kV and a current of 40mA. X-ray diffraction was applied for both phase identification as well as lattice spacing profiling. For phase analysis the scans were performed using a linear focus and Bragg-Brentano symmetrical geometry. The scattering angle range from 50 to 100º 2θ was recorded, using a step-size of 0.03º and measurement time per step of 5s. The measurements include the 111 and 200 reflections of (expanded) austenite.

To obtain the stress-depth profiles over the thickness of the gas-nitrided layer, the diffractometer was configured in asymmetric point focus mode with a fixed grazing incidence angle of α=2°. A vanadium window was used to remove Cr K_β radiation. It is common practice to apply high 2θ angle reflections for stress analysis. However, since the 220 and 311 reflections were very broad and had low intensity, only the 111 and 200 reflections could be used. These reflections of austenite and expanded austenite were included in all scans, ranging from 53 to 85º 2θ applying a step-size of 0.05º and a measurement time of 6s. Fig.1 gives the variation of the information depth as a function

of the effective ψ tilt in expanded austenite for the chosen measurement set up. Clearly, within the 2θ range investigated in the lattice strain investigations, the information depth changes by less than 1%.

The successive removal steps were realized by gently polishing the treated surface with a 3μm diamond suspension and monitoring the weight loss of the sample using an analytical balance. After each step the X-ray experiments were repeated.

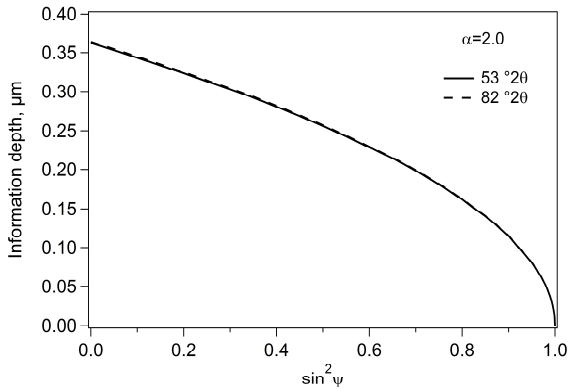

Figure 1 - Information depth in expanded austenite for grazing incidence X-ray diffraction at incident angle α=2, as a function of $\sin^2\psi$, for scattering angles of 53 and 82 º2θ.

Results and discussion

Figure 2 shows a light optical micrograph (Fig. 2a) and the Vickers hardness profile (Fig. 2b) of the sample nitrided at 430ºC for 20h in pure ammonia. The nitrided zone (Fig. 2a) exhibits the typical morphology of expanded austenite (γ_N) produced on austenitic stainless steels [2,3] and has a thickness of 13±1μm.

A hardness of around 1150HV is reached near the surface and maintained throughout the entire hardened zone. Approaching the case/core transition the hardness decreases abruptly to 220HV at about 13μm. The low substrate hardness is consistent with the supplied material condition.

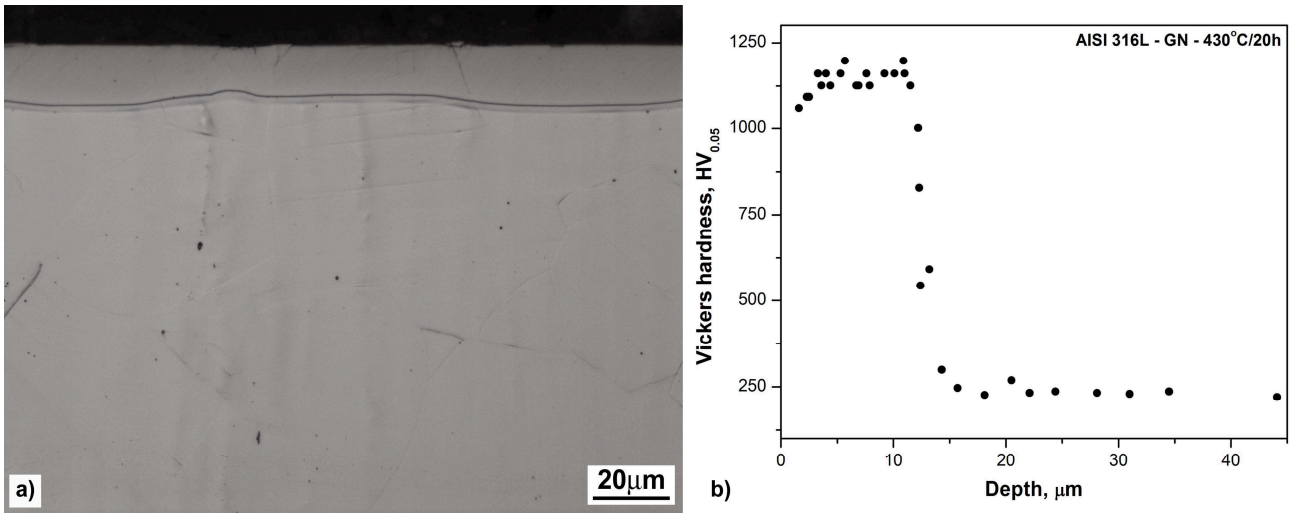

Figure 2 - (a) Reflected light micrograph and (b) Vickers hardness profile of AISI 316L steel gas nitrided at 430ºC for 20h.

Figure 3 presents the nitrogen-depth profile in atomic percentage (at.%) and a series of X-ray diffractograms obtained by applying the symmetric Bragg-Brentano geometry. The profile obtained by GDOES, shown on Fig. 3a, confirms the presence of a nitrogen-rich zone with a case/core transition that is consistent with Fig. 2.

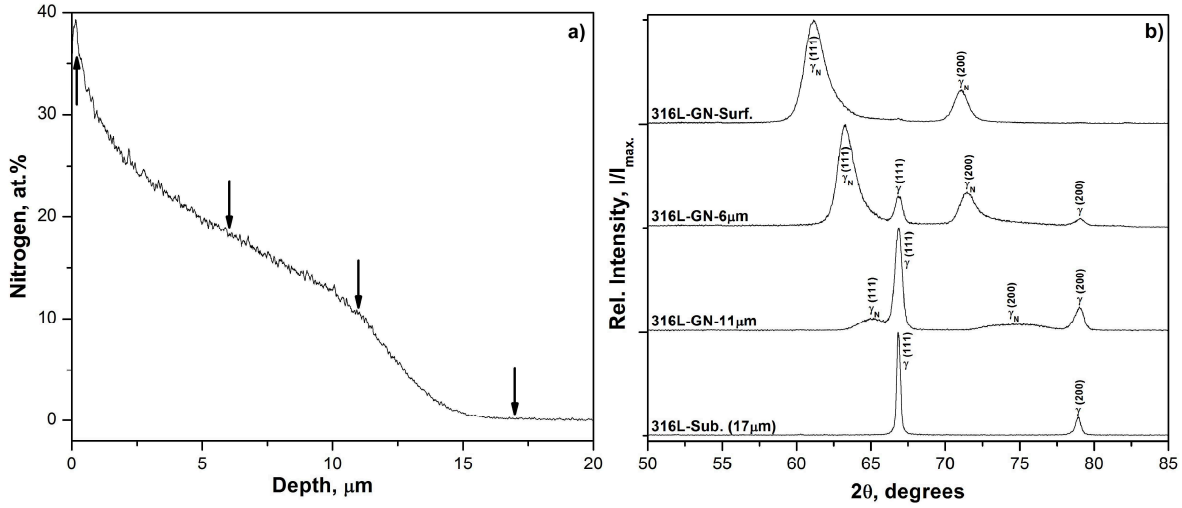

Figure 3 - (a) GDOES nitrogen profile; (b) X-ray diffractograms of the AISI 316L gas nitrided at 430ºC for 20h measured at the depths indicated by the arrows in the GDOES profile in (a).

Nitrogen reaches values as high as 35at.% at the surface and its concentration decreases steeply within 15μm. The case/core transition appears to extend over several microns as opposed to the hardness profile in Fig.2a. This is explained from a smearing of nitrogen profile and is inherent to sputter-depth profiling conditions applied in the GDOES technique and the variation in the thickness of the expanded austenite zone (cf. Fig. 2a). The arrows on the GDOES profile indicate the approximate positions where the XRD diffractograms in Fig. 3b were measured. The diffractograms show the 111 and 200 reflections for both austenite and expanded austenite in the 2θ range 50 to 85º. At the surface of the nitrided sample, where the nitrogen content is highest, the reflections are very broad and a large peak-shift to lower Bragg angle is observed as compared to untreated austenite. After removing 6μm by polishing the expanded austenite peaks shift to higher Bragg angles and additionally the 111 and 200 reflections from the underlying substrate appear, indicating that a diffracted intensity weighted average over the entire nitrided zone is obtained. At a depth of 6μm the nitrogen concentration is about 20 at.% according to the GDOES profile. After removal of 11μm, with only a few microns of expanded austenite left, the nitrogen content drops to10 at.% and the substrate peaks are very prominent. Interestingly, the 200 reflection of γ_N is very broad in this depth range. At a depth of 17μm the nitrided zone is removed entirely and only austenite reflections remain.

Figure 4 depicts the $\sin^2\psi$ plots measured at a fixed incidence angle α= 2° for the 111 (Fig. 4a) and 200 (Fig. 4b) reflections of the expanded austenite in a gas nitrided layer after performing consecutive sublayer removal through the nitrided case. The lattice spacing (d^{hkl}) values were calculated based on the centroid position of the 111 and 200 reflections and each curve from top to bottom on both figures represents a removal step of approximately 1μm. Near the case/core transition, the contribution of the substrate to the diffracted intensity was also included in determining the centroid peak position. It is observed that the lattice spacing changes significantly for all $\sin^2\psi$ curves and the analysis performed on the original surface gives the highest lattice spacing values.

As grazing incidence was employed, the probed lattice planes are actually tilted with respect to the surface normal even before the application of the χ tilt. The effective tilt angle ψ with respect to the surface normal is therefore:

$$\cos\psi = \cos\chi \cdot \cos(\theta - \alpha) \tag{1}$$

For the asymmetric grazing incidence geometry applied, the effective tilt angle (ψ) depends on the Bragg angle, 2θ (Eq. 1). Since the expanded austenite peak position changes with depth the sine

value of the effective tilt angle also changes with depth. Hence, the $\sin^2\psi$ dependencies in Fig. 4 are shifted to higher $\sin^2\psi$ with increasing depth.

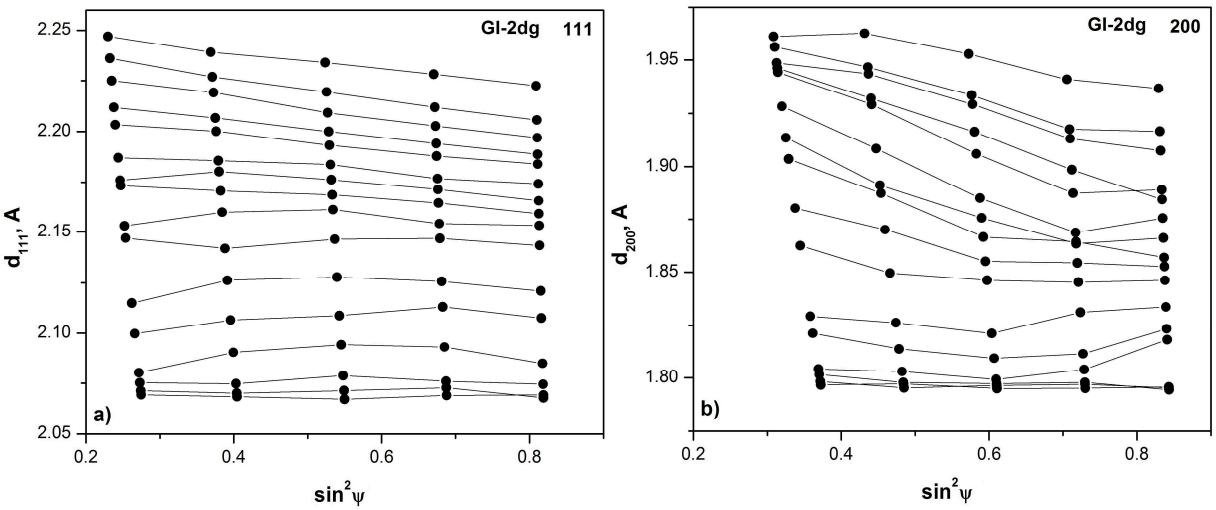

Figure 4 - $\mathrm{Sin}^2\psi$ plots for each of the removal steps performed on the gas nitrided AISI 316L for the: (a) 111 and (b) 200 expanded austenite reflections.

From the data in Fig. 4 both the stress values and the strain-free lattice parameter can be obtained for each removal step, provided that the XECs are known [12]. The results obtained with the XECs previously applied [3,6,10] and based on the single crystal elastic constants of austenitic stainless and the Kröner-Eshelby GIM are shown in Figures 5 and 6.

The lattice parameters, a_{hkl}, obtained from the lattice spacings of 111 and 200 reflections (Fig. 5a) decay with depth in a similar manner as observed for the nitrogen profile determined with GDOES profile (Fig. 3a). A constant value is reached at depths beyond the nitrided zone. Composition and lattice strain (macro-stresses, see below) are not the only features in the expanded austenite zone that affect the lattice parameter. The presence of nitrogen changes the stacking fault energy and the enormous residual stresses may locally, i.e. for relatively high nitrogen contents, exceed the yield strength, leading to dislocation generation and associated stacking faults. It is noted that nitrogen strengthens austenite considerably and, thus, a nitrogen concentration profile corresponds to a yield strength profile. The introduction of stacking faults leads to systematic shifts of the Bragg reflections, which are *hkl* dependent: the 111 peak shifts to higher Bragg angle and 200 to lower Bragg angle. The occurrence of a stacking fault density distribution may explain why the lattice parameter determined from the 200 reflection is systematically higher than for the 111 reflection in the surface adjacent depth region, where most plastic deformation is anticipated. At about 6 μm depth a cross-over occurs, such that a_{111} is systematically smaller than a_{200}. This systematic deviation at larger depth may indicate that the strain-free directions for 111 and 200 were not correct due to erroneous XECs.

Based on the average lattice parameter values from 111 and 200 reflections, shown in Fig. 5a, the nitrogen content vs. depth was estimated. The average lattice parameter was converted into nitrogen content (in at.%) using the equations determined for homogeneous expanded austenite produced on AISI 316 foils [3,8,9]. The graph in Fig. 5b shows a comparison of the thus obtained nitrogen contents and the nitrogen profile determined by GDOES (Fig. 3a). For high nitrogen contents, the equation of nitrogen expanded austenite was used, while for low contents, where no data exists for nitrogen expanded austenite [4], the equation for carbon expanded austenite was used. Taking into account that the XECs are most certainly incorrect, the satisfactory correspondence found between the nitrogen contents obtained by GDOES and the values estimated from the average strain-free lattice parameter, suggests that the strain-free directions for 200 and 111 are not affected to a large extent.

The obtained stress profiles for the two reflections studied are depicted in Fig. 6. The stresses resulting from analysis of 111 and 200 reflections are similar at the surface of the sample, about -3GPa. In both cases there is a maximum compressive stress value at some depth below the surface and appreciably higher stresses are observed for the 200 peak. It was already shown for expanded austenite that stress relief occurs at the surface by grain rotation and push-out [4-6]. Beyond the near surface region the stresses resulting from analysis of 111 and 200 reflections differ from each other by several GPa! Approaching the case/core transition similar tensile stresses are observed again. At the austenitic substrate constant and similar values are achieved.

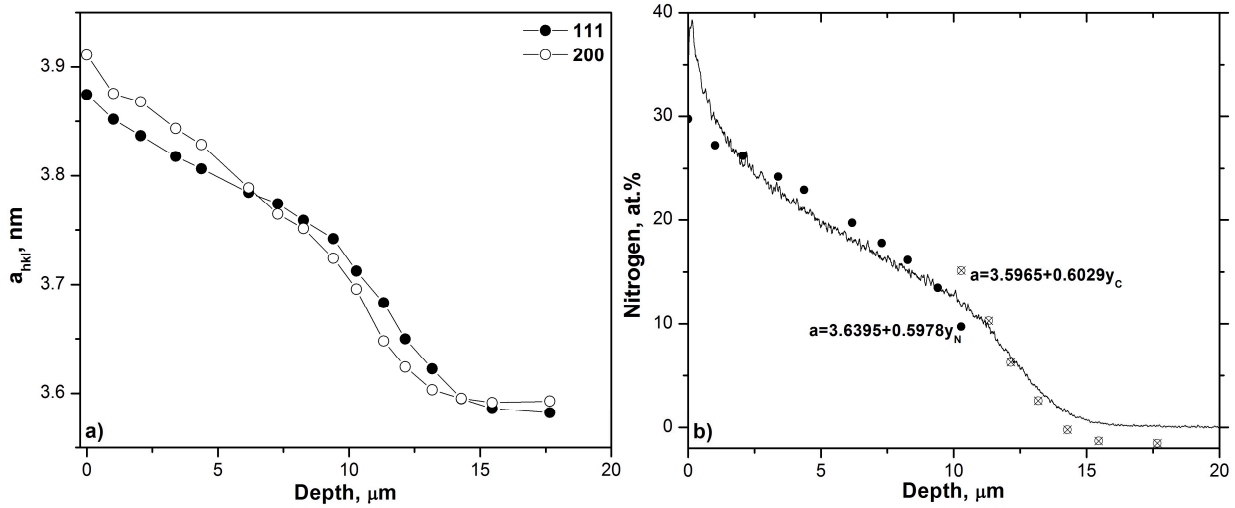

Figure 5 - (a) Lattice parameter (a^{hkl}) calculated from strain-free lattice spacing and (b) Comparison of the average lattice parameter from 111 and 200 reflections with the nitrogen profile from the GDOES analysis.

The striking discrepancy between stress values derived from $\sin^2\psi$ plots for 111 and 200 reflections is discussed as follows.

It can be ruled out that different ghost stresses for 111 and 200, arising from the lattice spacing gradient, combined with a variation in information depth [7,8,12], cause the discrepancy. GI-XRD was applied to limit the information depth. For the present case the information depth changes from 0.36 μm to 0.14 μm when $\sin^2\psi$ changes from 0 to 0.85, while it varies by less than 1% within the 2θ range, covering both 111 and 200, investigated (Fig.1). These shallow information depths and their variation over the 2θ range investigated are irreconcilable with a ghost stress (difference) of several GPas for the gradients observed. Instead, it is argued below that erroneous X-ray elastic constants (XECs) used for calculation of the stress from the lattice strain, are responsible for the observed discrepancy.

The stress value derived from the slope of the $\sin^2\psi$ plot depends strongly on the value of the XECs, S_1^{hkl} and S_2^{hkl}. These XECs can be obtained from single crystal elastic constants and an appropriate grain interaction model (GIM). For the present case the XECs of austenitic stainless steel were used, while the Kröner-Eshelby approach was used as the GIM. Indeed, a good correspondence between stresses derived from 111 and 200 is obtained beyond the nitrided zone where the sample is austenitic stainless steel (Fig. 6). Certainly, the presence of nitrogen in austenite affects the single crystal elastic constants. Recent nano-indentation work on expanded austenite demonstrated that the anisotropy of the *hkl* specific Young modulus, E_{hkl}, is changed radically [16]. For austenitic stainless steel AISI 316L $E_{111}>E_{200}$, while for expanded austenite on the same material $E_{111}<E_{200}$. It appears that this reversal of anisotropy is caused by an increase of E_{200} by about 30% [16]. Qualitatively, this would imply that using 200 for stress determination will lead to an overestimation of the residual stress. It is anticipated that the change in elastic constants depends on the interstitial content in expanded austenite.

Concerning the GIM applied, the Kröner-Eshelby model considers the crystallites probed with lattice strain measurement to be embedded in an elastically isotropic continuum in all directions, implying that the grains are relatively small as compared to the information depth. With the GI-XRD technique the information depth is very shallow as compared to the grain size and only the outer fraction of a micrometer of crystals at the surface is effectively probed. Consequently, more suitable GIM's should be sought for.

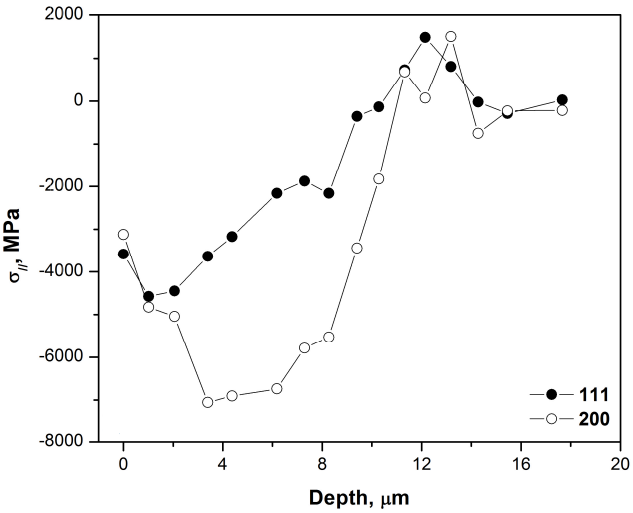

Figure 6 - Residual stress ($\sigma_{//}$) profiles, for the 111 and 200 reflections of expanded austenite.

Summary

The conducted experiments indicate that Grazing Incidence X-ray diffraction geometry is a feasible configuration for unraveling the steep interstitial and stress induced profiles resulting from nitrogen expanded austenite. A good correspondence between the lattice parameter determined in the strain free direction and the nitrogen profile from GDOES is found. Large compressive stresses occur in expanded austenite and distinct stress values are obtained for both 111 and 200 reflections. The discrepancy between stress values determined from lattice strains for different *hkl* is explained from a change of the X-ray elastic constants with nitrogen content, leading to a reversal of anisotropy. Furthermore it is argued that the Kröner-Eshelby Grain Interaction Model is inappropriate for the present case of a shallow information depth as compared to the grain size.

References

[1] Z.L. Zhang, T. Bell, *Surf. Eng.* 1 (1985) 131-136.
[2] T. Christiansen, M.A.J. Somers, *Surf. Eng.* 21 (2005) 445-455.
[3] T.L. Christiansen, M.A.J. Somers, *Int. J. Mater. Res.* 100 (2009) 1361-1377.
[4] T. Christiansen, M.A.J. Somers, *Metall. Mater. Trans. A* 37 (2006) 675-682.
[5] J.C. Stinville, C. Templier, V. Villechaise, L. Pichon, *J. Mat. Sci.* 46 (2011) 5503-5511.
[6] J.C. Stinville, P. Villechaise, C. Templier, J.P. Rivière, M. Drouet, *Acta Mater.* 58 (2010) 2814-2821.
[7] T.L. Christiansen, M.A.J. Somers, *Metall. Mater. Trans. A* 40 (2009) 1791-1798.
[8] T. Christiansen, M.A.J. Somers, *Mater. Sci. Eng. A* 424 (2006) 181-189.
[9] T.L. Christiansen, T.S. Hummelshøj, M.A.J. Somers, *Surf. Eng.* 26 (2010) 242-247.
[10] S. Jegou, T.L. Christiansen, M. Klaus, Ch. Genzel, M.A.J. Somers, *Thin Solid Films* 530 (2013) 71-76.
[11] M. Meixner, M. Klaus, Ch. Genzel, *J. Appl. Cryst.* 46 (2013) 610-618.
[12] M.A.J. Somers, E.J. Mittemeijer, *Metall. Mater. Trans. A* 21 (1990) 189-204.
[13] F. Bollenrath, V. Hauk, E.H. Muller, *Z. Metallkd.* 58 (1967) 76-82.
[14] K. Salmutter, F. Stangler, *Z. Metallkd.* 51 (1960) 544-548.
[15] V. Hauk, H. Kockelmann, *Arch. Eisenhüttenwes.* 31 (1976) 38-41.
[16] J.C. Stinville, C. Tromas, P. Villechaise, C. Templier, *Scr. Mater.* 64 (2011) 37-40.